# REPORT DOCUMENTATION PAGE

*Form Approved*
*OMB No. 0704-0188*



**PLEASE DO NOT RETURN YOUR FORM TO THE ABOVE ORGANIZATION.**

| 1. REPORT DATE *(DD-MM-YYYY)* | 2. REPORT TYPE | 3. DATES COVERED *(From - To)* |
|---|---|---|
| 11/04/2015 | Journal Article | |

**4. TITLE AND SUBTITLE**

Galvanic Couple Current and Potential Distribution between a Mg Electrode and 2024-T351 under Droplets Analyzed by Microelectrode Arrays

**5a. CONTRACT NUMBER**

**5b. GRANT NUMBER**

**5c. PROGRAM ELEMENT NUMBER**

0602435N

**6. AUTHOR(S)**

A. D. King, Jason. S. Lee, and J. R. Scullya

**5d. PROJECT NUMBER**

**5e. TASK NUMBER**

**5f. WORK UNIT NUMBER**

73-4635-04-5

**7. PERFORMING ORGANIZATION NAME(S) AND ADDRESS(ES)**

Naval Research Laboratory
Oceanography Division
Stennis Space Center, MS 39529-5004

**8. PERFORMING ORGANIZATION REPORT NUMBER**

NRL/JA/7330-14-2175

**9. SPONSORING/MONITORING AGENCY NAME(S) AND ADDRESS(ES)**

Office of Naval Research
One Liberty Center
875 North Randolph Street, Suite 1425
Arlington, VA 22203-1995

**10. SPONSOR/MONITOR'S ACRONYM(S)**

ONR

**11. SPONSOR/MONITOR'S REPORT NUMBER(S)**

**12. DISTRIBUTION/AVAILABILITY STATEMENT**

Approved for public release, distribution is unlimited.

**13. SUPPLEMENTARY NOTES**

**14. ABSTRACT**

The galvanic throwing power of bare and polymer coated Mg over a simulated bare AA2024 scribe was studied directly with diagnostic multi-electrode arrays, which enable the spatial distribution of cathodic current density to be elucidated. The galvanic current density over the AA2024-T351 coupled to Mg in various full immersion, thin layer, and droplet electrolyte geometries relevant to atmospheric field exposures was investigated during simulated atmospheric exposures. In these microelectrode studies, current and potential distributions extended somewhat more uniformly across a 5.75 mm long, simulated bare 2024-T351 scratch when the electrolyte layer was thick, continuous and more ionically conductive (i.e., higher salt concentration) in the absence of a polymer coating over the Mg. Current and potential distributions did not extend across simulated defects when the electrolyte became discontinuous or the ionic path became tortuous due to drying or the addition of a resistive polymer coating over the Mg. Additionally, galvanic protection is shown to intensify for short period of time during drying and re-wetting cycles at close distances between Mg and 2024-T351 rationalized to be caused by changing electrolyte conductivity, E-i behavior, and electrode area effects. The drying characteristics of individual salts were also shown to have an effect on the current and potential distribution as $MgCl_2$ (due to its low deliquescence/efflorescence point of ~35% RH at STP) was shown to be less susceptible to drying at low RH, thus extending the time into the drying cycle where the galvanic couple was active compared to pure NaCl or ASTM Substitute Ocean Water.

**15. SUBJECT TERMS**

galvanic couple current; microelectrode arrays

| 16. SECURITY CLASSIFICATION OF: | | | 17. LIMITATION OF ABSTRACT | 18. NUMBER OF PAGES | 19a. NAME OF RESPONSIBLE PERSON |
|---|---|---|---|---|---|
| a. REPORT | b. ABSTRACT | c. THIS PAGE | | | Jason S. Lee |
| Unclassified | Unclassified | Unclassified | UU | 12 | 19b. TELEPHONE NUMBER *(Include area code)* (228) 688-4494 |

Reset

# PUBLICATION OR PRESENTATION RELEASE REQUEST

14-1231-1743 Pubkey 9264 NRLINST 5600.2

Ref: (a) NRL Instruction 5600.2
(b) NRL Instruction 5510.40D

Encl: (1) Two copies of subject paper (or abstract)

( ) Abstract only, published
( ) Book
( ) Conference Proceedings (refereed)
( ) Invited speaker
(X) Journal article (refereed)
( ) Oral Presentation, published
( ) Other, explain

( ) Abstract only, not published
( ) Book chapter
( ) Conference Proceedings (not refereed)
( ) Multimedia report
( ) Journal article (not refereed)
( ) Oral Presentation, not published

STRN NRL/JA/7330-14-2175
Route Sheet No. 7330/
Job Order No. 73-4635-04-5
Classification X U
Sponsor ONR BCA/W
approval obtained ___ yes X no

Title of Paper or Presentation

**Galvanic Couple Current and Potential Distribution Between a Mg Electrode and 2024-T351 Analyzed by Microelectrode Arrays and Finite Element Analysis**

Author(s) Name(s) (*First,MI,Last*), Code, *Affiliation if not NRL*

**A. D. King** Univ. of Virginia **Jason S. Lee** 7332 **J. R. Scully** Univ. of Virginia

It is intended to offer this paper to the _____
(*Name of Conference*)

_____
(*Date, Place and Classification of Conference*)

and/or for publication in **Journal of Electrochemical Society, Unclassified**
(*Name and Classification of Publication*) (*Name of Publisher*)

After presentation or publication, pertinent publication/presentation data will be entered in the publications data base, in accordance with reference (a).
It is the opinion of the author that the subject paper (is ____ ) (is not ___X_) classified, in accordance with reference (b).
This paper does not violate any disclosure of trade secrets or suggestions of outside individuals or concerns which have been communicated to the Laboratory in confidence. This paper (does ____ ) (does not ___X_) contain any militarily critical technology.
This subject paper (has ____ ) (has never _X_ ) been incorporated in an official NRL Report.

**Jason S. Lee, 7332** _____
Name and Code (*Principal Author*) (Signature)

| CODE | SIGNATURE | DATE | COMMENTS |
|---|---|---|---|
| Author(s) Lee | | 5/15/14 | Need by 04 Jun 14 |
| | | | Publicly accessible sources used for this publication |
| | | | |
| | | | This is a Final Security Review. Any changes made in the document, after approved by Code 1231, nullify the Security Review. |
| Section Head Teague | | 5/16/14 | |
| Branch Head **Richard L. Crout, 7330** | | 5-19-2014 | |
| Division Head **Ruth H. Preller, 7300** | | 5/19/14 | 1. Release of this paper is approved.<br>2. To the best knowledge of this Division, the subject matter of this paper (has ____ ) (has never _X_ ) been classified. |
| Security, Code **1231** | | 5/27/14 | 1. Paper or abstract was released.<br>2. A copy is filed in this office. |
| Office of Counsel,Code **1008.3** | | 6/3/14 | |
| ADOR/Director NCST **E. R. Franchi, 7000** | | | |
| Public Affairs (*Unclassified/Unlimited Only*), Code **7030.4** | Shannon Mewi | 6-2-14 | S |
| Division, Code | | | |
| Author, Code | | | |

HQ-NRL 5511/6 (Rev. 12-98) (e) THIS FORM CANCELS AND SUPERSEDES ALL PREVIOUS VERSIONS

*Journal of The Electrochemical Society*, **162** (1) C12-C23 (2015)
0013-4651/2015/162(1)/C12/12/$31.00 © The Electrochemical Society

# Galvanic Couple Current and Potential Distribution between a Mg Electrode and 2024-T351 under Droplets Analyzed by Microelectrode Arrays

**A. D. King,[a,z] J. S. Lee,[b,*] and J. R. Scully[a,**]**

[a]*Department of Materials Science and Engineering, University of Virginia, Charlottesville, Virginia 22904, USA*
[b]*US Naval Research Laboratory, Stennis Space Center, Mississippi 39529, USA*

The galvanic throwing power of bare and polymer coated Mg over a simulated bare AA2024 scribe was studied directly with diagnostic multi-electrode arrays, which enable the spatial distribution of cathodic current density to be elucidated. The galvanic current density over the AA2024-T351 coupled to Mg in various full immersion, thin layer, and droplet electrolyte geometries relevant to atmospheric field exposures was investigated during simulated atmospheric exposures. In these microelectrode studies, current and potential distributions extended somewhat more uniformly across a 5.75 mm long, simulated bare 2024-T351 scratch when the electrolyte layer was thick, continuous and more ionically conductive (i.e., higher salt concentration) in the absence of a polymer coating over the Mg. Current and potential distributions did not extend across simulated defects when the electrolyte became discontinuous or the ionic path became tortuous due to drying or the addition of a resistive polymer coating over the Mg. Additionally, galvanic protection is shown to intensify for short period of time during drying and re-wetting cycles at close distances between Mg and 2024-T351 rationalized to be caused by changing electrolyte conductivity, E-i behavior, and electrode area effects. The drying characteristics of individual salts were also shown to have an effect on the current and potential distribution as $MgCl_2$ (due to its low deliquescence/efflorescence point of ∼35% RH at STP) was shown to be less susceptible to drying at low RH, thus extending the time into the drying cycle where the galvanic couple was active compared to pure NaCl or ASTM Substitute Ocean Water.


Manuscript submitted May 23, 2014; revised manuscript received October 23, 2014. Published November 11, 2014.

A commercial organic coating system containing an Mg-pigmented polymer primer (Mg-rich primer, MgRP) has been developed for the corrosion protection of aluminum alloys, such as precipitation age hardened 2024-T351, and has performed well in field studies.[1–13] The MgRP is designed to be applied to an aluminum alloy substrate as a primer layer, above any pretreatments, but below any topcoats which may be used. The MgRP is designed to galvanically couple the Mg pigment in the primer to the substrate and provide sacrificial anode based cathodic protection to the aluminum alloy (AA2024-T351).[2,5,8] When coupled to the AA2024-T351 (or similar alloy) substrate, the Mg pigment becomes an electron donor, and mixed potential theory can be used to explain the galvanic couple potential of the MgRP/AA2024-T351 system when exposed to full immersion. Results in the literature support the notion of mixed potential theory describing the galvanic coupling behavior between the primer and substrate.[1,3–7,14,15]

The galvanic couple potential sensed at a given location on an anode (Mg pigment) or cathode (AA2024-T351) will depend on the geometric arrangement of the anode and cathode, the surface area ratio between the two electrodes exposed to immersion, the E-i electrochemical kinetics, as well as other factors such as any electrical and ionic resistances that may exist between the anode and cathode.[8] The Mg pigment volume concentration (PVC) will affect both the resistive paths through the organic coating between the Mg pigment and the underlying AA2024-T351 substrate as well as the path through the organic coating and the electrolyte above and through the overlying electrolyte to any exposed AA2024-T351.[8] All of these factors will mediate the galvanic couple potential existing along each metal surface even in the case of a uniform current distribution between anode and cathode, for instance in a simple parallel plate arrangement.

A critical issue with regards to predicting MgRP's protection capabilities in the field is developing a means for predicting the throwing power or spatial current and potential distribution of the physical MgRP/AA2024-T351 system. The typical geometry here is not the parallel plate arrangement but a coating in the same plane as a thin rectangular scratch. The distance over which the MgRP coating system can protect a scratch or defect exposing bare AA2024-T351 by sacrificial anode based cathodic protection, is hereafter termed the "galvanic throwing power". This is the perpendicular distance into the scratch over which cathodic protection is afforded. This arrangement has been studied before in the case of aluminum alloys.[16–20] Conversely, the term hereafter called the "inverse galvanic throwing power" is the distance into the MgRP coating in which Mg pigment is anodically polarized while actively galvanically coupled to the AA2024-T351 scribe, scratch, or defect. A question remains in the literature as to whether a discernable region of increased Mg pigment depletion exists along the edges of a defect or scratch due to such an inverse throwing power. Understanding and predicting the throwing power and inverse throwing power of a sacrificial coating such as MgRP is complicated because the scribe size, coating formulation, electrolyte composition, electrolyte geometry, and bare/coated area ratios can all, in theory, be limiting factors when considering protection ability or throwing power of a coating that protects by sacrificial anode based galvanic protection. In this paper, the importance of some of these factors is addressed.

The thermodynamic equilibrium concentration of a given electrolyte varies with ambient RH.[21–23] As a given deposited hygroscopic salt deliquesces on a surface it will, over time, equilibrate with the ambient RH to form an electrolyte layer or droplet of equilibrium concentration. A hypothetical RH cycle which could be observed in an environmental exposure is depicted in Figure 1. As the RH in an exposure environment changes with time, so does the equilibrium salt concentration and thus ionic conductivity, as well as thickness of the electrolyte layer (also shown Figure 1 assuming an infinite planar geometry). These are important factors controlling the galvanic throwing power and subsequent cathodic protection vs. scratch distance afforded by the MgRP coating system.

A large source of variation between performance of the coating in the salt fog and field exposure environments, with regards to throwing power, is the electrolyte geometry in each environment. A sacrificial coating can only galvanically protect defects (or bare substrate at scratches) which it is both electrically and ionically connected to by a continuous path. Across exposure environments such as artificial environment like ASTM B-117 salt fog, in a rainstorm with large drops, during a dewing event, or during wetting and drying cycles due to changing ambient RH, both the electrolyte concentration and geometry will vary dramatically from thick and continuous to thin and tortuous, and even isolated droplets.

One method to characterize the throwing power has been post-exposure characterization. Such characterization has been conducted

*Electrochemical Society Active Member.
**Electrochemical Society Fellow.
[z]E-mail: adk3m@virginia.edu

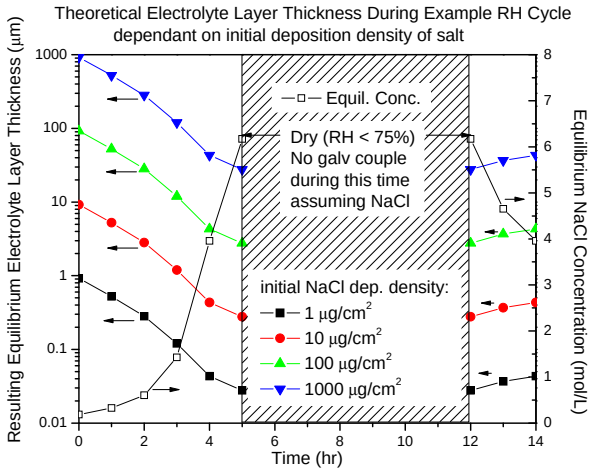


**Figure 1.** Hypothetical RH cycle and resulting electrolyte layer thickness for various NaCl surface deposition densities assuming an infinite planar electrolyte.

on scribes of environmentally exposed test panels. Calcareous deposits, primarily consisting of $CaCO_3$, along with Mg deposits, are indicative of regions of cathodic protection afforded to the AA2024-T351 by the MgRP.[24–31] An attempt was made to examine the throwing power after exposure in the laboratory and field by obtaining EDS of the bare scribe. In past field studies of the MgRP coating system, definitive determination of throwing power by post-exposure sample evaluation was difficult and only moderately successful.[12,13]

For these reasons, there exists a critical need in the literature to directly assess and measure the throwing power of the MgRP system. The objective of this study to utilize instrumented electrode arrays to quantitatively observe the spatial distribution of current density over a model Mg/AA2024-T351 galvanic couple, with and without a polymer coating over the Mg, under various environmental conditions and to gain a better understanding of the evolution of the galvanic throwing power as a function of variables described above. Moreover, a secondary goal is to define some of the attributes that promote uniform current and potential distribution across the scribe.

A separate work will utilize FEA software (COMSOL), in conjunction with experimentally obtained electrochemical boundary conditions of Mg, AA2024-T351, and the MgRP coating system under relevant chemical conditions, to develop a fully functional, physically representative model. The model will be developed in an effort to accurately predict the galvanic throwing power of the MgRP coating system as a function of coating parameters, physical conditions, as well as environment.

## Experimental

*Materials.*— 99.9% magnesium rod (8.0 mm diam.), 500 μm diameter 99.9% magnesium wire, 1.6 mm thick AA2024-T351 sheet, and 254 μm diameter AA2024-T4 wire were studied in these investigations. Table I and Table II show the chemical analysis of both the AA2024 and the Mg used in this work. Chemical analysis shows the Mg rod and wire had a measured purity of over 99.9% and is substantially similar to the powder used in commercial Mg-Rich Primer (MgRP) products.[8] The AA2024-T4 wire was insulated with a 25 μm thick polyimide coating making the total wire diameter approximately 300 μm. The Mg rod was mounted in EpoThin epoxy resin manufactured by Buehler in order to make clamping the sample to an electrochemical flat cell easier. The bare electrodes were prepared by alternating abrasion with silicon-carbide paper and rinsing with 18.2 MΩ deionized water to a final polishing grit of 1200. The samples were then dried with laboratory tissue before use.

*Full immersion electrochemical analysis to establish boundary conditions.*— Potential control during electrochemical experiments was maintained using a potentiostat with computer interface software. Solartron 1287A/1255B and Gamry Reference 600 potentiostats were selected because they enable electrochemical impedance spectroscopy (EIS) measurements along with traditional electrochemical measurements. Saturated Calomel reference electrodes (SCE) were used in full immersion testing.

Anodic potentiodynamic scans were conducted on 99.9% pure, 8.0 mm diameter bare Mg electrodes. The tests were run in various bulk solutions of quiescent NaCl and $MgCl_2$ with ambient aeration as well as NaCl pre-saturated with $Mg(OH)_2$. The potentiodynamic scans were conducted after 10 minutes at the open circuit potential (OCP). A typical anodic scan started at −0.2 V vs OCP up to +0.7 V vs. OCP and scanned at 1.0 mV per second. Cathodic scans were conducted on 2024 at various boundary layer thicknesses using thin cells, full immersion, wires and RDE. A typical cathodic scan started at +0.2 V vs OCP and scanned down to −1.0 V vs. OCP at 0.1667 mV per second. In the literature, Cheng and Jakab both show that as thickness goes from 2000 to 100 μm, the limiting current density for the oxygen reduction reaction (ORR) on AA2024 only increases by a factor of two at about −1.0 V vs SCE.[32,33]

*Multichannel microelectrode galvanic array.*— A microelectrode array consisting of one 500 μm diameter, flush mounted 99.9% Mg electrode and twenty isolated, 254 μm diameter, flush mounted AA2024-T4 electrodes (300 μm total diameter including polyimide insulation) was arranged in a single straight line (∼6 mm wide) and flush mounted in EpoThin epoxy resin to diagnostically represent the MgRP/AA2024 galvanic couple system extending perpendicular to a scribe or scratch. The array simulates the bare AA2024-T351 perpendicular to the scribe length and parallel to the scratch width from the edge of the primer. An optical micrograph of the microelectrode array is shown in Figure 2. The spacing between electrodes was approximately 30 – 50 μm (Figure 2). A Scribner model MMA910B was used to provide a graphical interface and data acquisition of each microelectrode current. The MMA 910B is capable of galvanically coupling and measuring up to 100 working electrode current channels and contains an individual zero resistance ammeter (ZRA) on each current channel with a measureable current range of 3.3 nA to 100 μA per channel. It is important to note that neither a counter electrode nor reference electrode was used in this study as only localized galvanic currents were obtained. The throwing power of the Mg across the AA2024-T4 array is often depicted spatially in this paper by either plot of i ($A/cm^2$) vs. position or a blue/red color map at various times of interest. The minimum current limit of the multichannel multielectrode analyzer is approximately $1 \times 10^{-9}$ A and the maximum is

**Table I. Composition of AA2024-T351 used as a bare electrode in these investigations. Compositions provided by QUANT Quality Analysis and Testing Corporation in wt%.**

| AA2024 | Al | Cu | Mg | Mn | Fe | Zn | Si | Ti | Cr | V |
|---|---|---|---|---|---|---|---|---|---|---|
| T351 Sheet | Balance | 4.56 | 1.26 | 0.59 | 0.22 | 0.12 | 0.08 | 0.02 | 0.01 | 0.01 |
| T4 Wire | Balance | 4.35 | 1.36 | 0.62 | 0.5 | 0.25 | 0.5 | 0.15 | 0.1 | NR |

**Table II. Compositions of Mg Rod (99.9%) purchased from Alfa Aesar. All compositions reported in wt.%. (Mg: Balance). Compositions provided by QUANT Quality Analysis and Testing Corporation. NR: Not Reported.**

| element | Si | Al | Fe | Cu | Zn | Mn | Ni | Zr | Pb | Sn | C | S | O |
|---|---|---|---|---|---|---|---|---|---|---|---|---|---|
| rod/wire | NR | 0.02 | 0.008 | 0.003 | 0.03 | <0.01 | <0.001 | <0.01 | NR | NR | <0.001 | <0.001 | 0.001 |

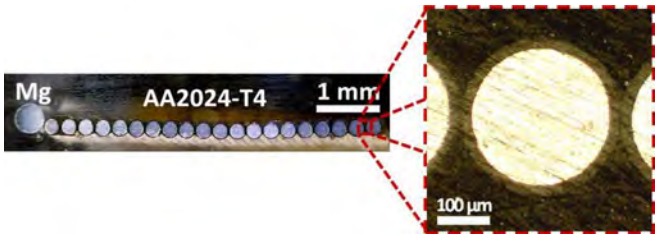


**Figure 2.** Optical images of the bare Mg/AA2024-T4 microelectrode array used to diagnostically assess the throwing power of Mg over a representative bare AA2024-T4 scratch in an RH controlled cabinet. The Mg electrode is 500 μm in diameter. The AA2024-T4 electrodes are 254 μm in diameter insulated by a 25 μm thick polyimide coating with a mean electrode spacing of 50 μm. The total width of all of the AA2024-T4 microelectrodes is approximately 5750 μm and the total area ration of AA2024:Mg is 5:1.

$1 \times 10^{-4}$ A, resulting in (due to the cross-sectional area of the flush mounted microelectrodes) minimum and maximum measurable current densities of $2 \times 10^{-6}$ A/cm$^2$ and $2 \times 10^{-1}$ A/cm$^2$. In each color map, dark red indicates an anodic current $\geq 1 \times 10^{-5}$ A/cm$^2$ and dark blue indicates a cathodic current of $\leq -1 \times 10^{-5}$ A/cm$^2$. Microelectrodes which are freely corroding (e.g., anodes and cathodes present on one electrode) pass a net current of zero and are color coded white.

In three separate experiments, approximately 40 μL of 1) 0.9 M NaCl solution, 2) 0.6 M $MgCl_2$ solution, and 3) ASTM Substitute Ocean Water (SOW) solution were each applied in a thin layer to the top of the microelectrode galvanic array such that the electrolyte covered every electrode in the array. The height of the as-applied, thin layer electrolyte film was measured with a digital multimeter and vertical digital caliper setup to be approximately $500 \pm 100$ μm thick at the center for each experiment. The array was then placed in the relative humidity controlled cabinet and electrically connected to the MMA. Over the course of 6 hours, the relative humidity in the cabinet was cycled from ambient RH to low RH (<20%), up to high RH (>90%) and back to low RH (< 20%) and recorded in order to observe the effect of a wet/dry cycle on the throwing power of the single Mg electrode over the AA2024 microelectrodes under the intial 0.9 M NaCl solution, 0.6 M $MgCl_2$ solution, and ASTM Substitute Ocean Water solution.

In a fourth set of experiments, a clear, quick-drying acrylic polymer was applied to the surface of the Mg electrode in the Mg/AA2024-T4 microelectrode array in order to mimic the high ionic resistance of the primer polymer in the MgRP coating system. Electrochemical impedance measurements on the acrylic polymer were obtained for comparison to that of MgRP coated (with $PVC_{Mg} = 45\%$) AA2024-T351. The EIS measurements were obtained utilizing a traditional full immersion, three electrode cell and FRA/potentiostat setup in 0.9 M NaCl, utilizing the Mg wire in the microelectrode array as the working electrode, a commercial SCE reference electrode, and a Pt mesh counter electrode. The low frequency impedance ($\sim 4 \times 10^6\ \Omega \cdot$ cm$^2$), saddle frequency ($\leq$0.01 Hz), and breakpoint frequency ($\sim$3 Hz) for the quick drying acrylic polymer were similar to that of the MgRP coating over AA2024-T351 making it a suitable analog to simulate the ionic resistance added by the MgRP polymer to the MgRP/AA2024-T351 galvanic couple system for the purpose of studying throwing power.[34–40]

In additional experiments, 10, 100, 250, and 1000 μg/cm$^2$ of both NaCl and ASTM Substitute Ocean Water salts were applied to the surface of the bare Mg/bare AA2024-T4 microelectrode array. The salts were applied using a spray bottle application method in which a known concentration of electrolyte was sprayed from a spray bottle at a constant distance from the samples surface in an enclosed chamber. The average deposition volume per spray using this specific setup was characterized and calibrated by both rinsed-solution conductivity measurements and weight gain measurements. Using the known deposition volume per spray and the known electrolyte concentration in the spray bottle, a desired salt deposition density was applied to the array's surface. After depositing the electrolyte of interest onto the array, the array was placed into an RH controlled cabinet which had been purged with dry air (RH $\approx$ 10%) to quickly dry the electrolyte droplets. The size of the electrolyte droplets applied by the spray bottle method were characterized by optical analysis with computational image analysis software (ImageJ) and had a mean diameter of approximately 160 μm $\pm$ 60 μm. The mean diameter of the applied droplets, within one standard deviation, was larger than the microelectrode array inter-electrode spacing of 50 μm (spacing shown in Figure 2).

The total of the net cathodic current passing through each AA2024-T4 microelectrode was found to be equal in magnitude and opposite in sign to the total anodic current passing through the galvanically coupled Mg microelectrode confirming that the galvanic interaction between the Mg and AA2024-T351 microelectrodes was in accordance with mixed potential theory and that instrumentation currents were below the detection limit. The residual "instrument" noise of the entire microelectrode array under dry conditions remained $0 \pm 200$ nA throughout the length of the experiment.

*Instrumented relative humidity controlled cabinet.*— The microelectrode array was housed in an instrumented, relative humidity controlled cabinet. The ribbon cable connections were made to the MMA900B via a feed through in the wall of the cabinet. The RH controlled cabinet was produced from a Plas-Labs desiccator cabinet (PN: 861-CG) and is shown schematically in Figure 3. The cabinet was instrumented with an OMEGA OM-EL-USB-2-LCD-PLUS RH and temperature data logger and a DINO-LITE AD7013MT USB microscope utilized for time lapse imaging. RH was controlled via the

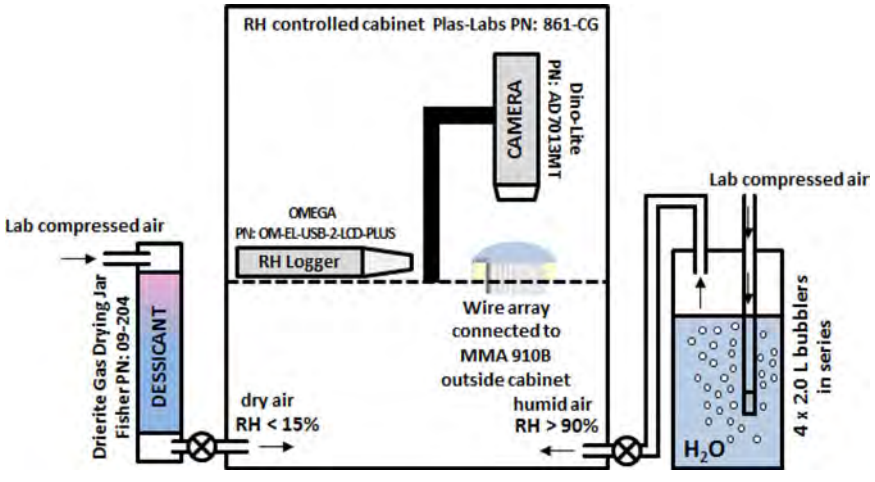


**Figure 3.** Schematic illustration of RH controlled cabinet and camera setup used to environmentally expose Mg/AA2024-T4 microelectrode arrays to high and low RH.

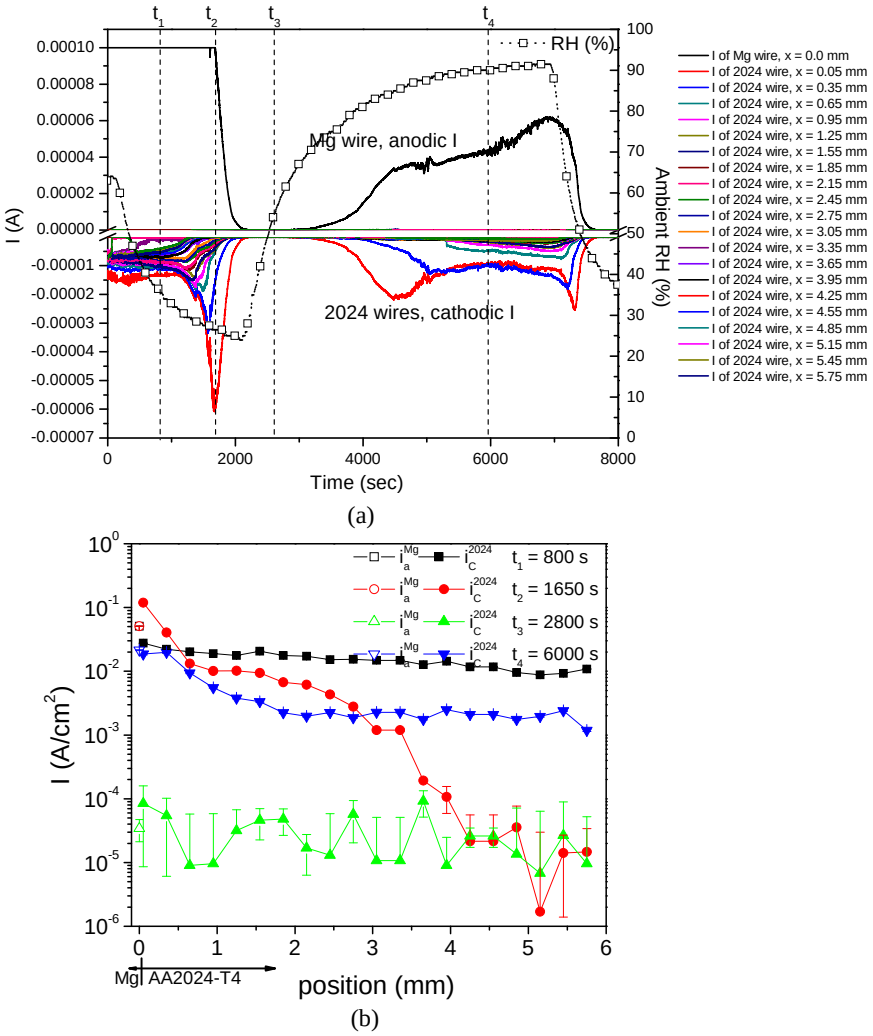


**Figure 4.** (a) Measured current and RH vs. time through each electrode and (b) average current density vs. position on the bare Mg/AA2024-T4 microelectrode array during an episodic wetting and drying event under 0.9 M NaCl.

flow of dry or humid air into the chamber. Humid air was produced by passing house compressed air through a series of four 2 L $H_2O$ diffuser bubblers, achieving an ambient RH of up to 95%. Dry air was produced by passing house air through Drierite gas drying jars, achieving an ambient RH of as low as 10%.

*Results.—Throwing power (TP) experimentally measured by a coupled electrode multichannel microelectrode array under continuous thin layer electrolytes during wetting and drying.—* Under both a 500 ± 100 μm thick layer of 0.9 M NaCl (Figure 4) and similar thickness layer of ASTM Substitute Ocean Water (Figure 5) covering the entire 5750 μm microelectrode array, the cathodic polarization provided by the Mg electrode was initially observed to spread across the entire width of the AA 2024 array indicating a TP greater than or equal to 5750 μm. This is indicated by a net cathodic current density greater than $10^{-6}$ A/cm$^2$ sensed by the AA2024-T4 extending to the last AA2024-T4 electrode in the array (at a position = 5.75 mm) in Figure 4b and Figure 5b, respectively. $H_2$ bubbles produced by increased hydrogen evolution were observed to actively form on each cathodically polarized AA2024-T351 electrode in the array. Upon lowering the cabinet RH to less than 20%, the electrolyte layer was visually observed to decrease in thickness and area of coverage ($t_2$ in Figure 4b) and salt was continuously deposited at the periphery of the inward shrinking electrolyte layer until the array was completely dry ($t_3$ in Figure 4b). As the electrolyte layer decreased in thickness and radius, the throwing power of the Mg electrode decreased from the full width of the array ($t_1$ in Figure 4b) to zero ($t_3$ in Figure 4b and Figure 5b) indicating cessation in sacrificial galvanic protection of the AA2024-T4 electrodes by the Mg electrode. During drying, the net cathodic current density on the individual AA2024-T4 electrodes closest to the Mg electrode (x = 50 μm) was observed to increase to a peak (at time $t_2$ in Figure 4b and Figure 5b) presumably due to the combined effects of the increasing electrolyte concentration and the decreasing area of the active cathode relative to a fixed anode. At time $t_2$ during drying under NaCl ($t_2$ in Figure 4a), the AA2024-T4 electrode at x = 50 μm had a cathodic current density of $-1.2 \times 10^{-1}$ A/cm$^2$ corresponding to a local interfacial potential of approximately $-1.5$ $V_{SCE}$ (determined from Figure 6b),[c] a distant AA2024-T4 electrode at x = 2.75 mm had a cathodic current density of $-1.6 \times 10^{-4}$ A/cm$^2$ corresponding to a local interfacial potential of $-1.3$ $V_{SCE}$, and the farthest AA2024-T4 electrode at x = 5.75 mm had a steady net current density of zero indicating the electrode was not protected by Mg and either freely corroding (at OCP) or dry. After $t_2$, the net cathodic current density on the AA2024-T4 electrodes closest to the Mg electrode were then observed to decrease in magnitude to zero as the effect of the increasingly thin and tortuous electrolyte geometry reduced the ionically conductive path despite the increase in concentration of NaCl.

[c]The E-log i curve in Figure 6 is for bulk immersion with an ORR diffusional boundary layer that may differ from the array/droplet configuration. However, Jakab and Cheng show that as water layer thickness varies from 2000 to 100 um, $i_L$ for ORR on 2024-T3 only increases by a factor of 2 at about −1.0 V SCE. At or below about −1.2 V SCE the difference in $O_2$ boundary layer thickness does not effect HER which is charge transfer controlled.[32,33]

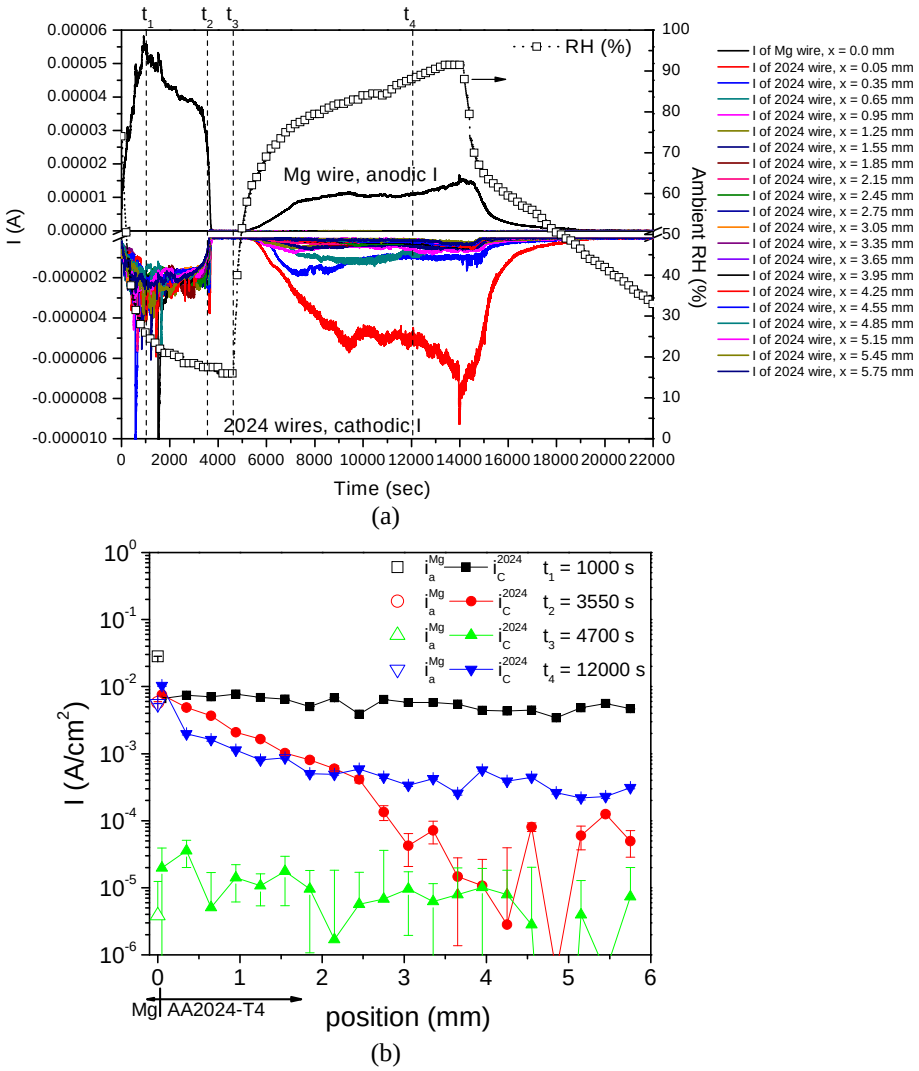


**Figure 5.** (a) Measured current and RH vs. time through each electrode and (b) average current density vs. position on the bare Mg/AA2024-T4 microelectrode array during an episodic wetting and drying event under ASTM Substitute Ocean Water.

Upon increasing the RH in the cabinet to approximately 93% the electrolyte layer ($t_4$ in Figure 4b and Figure 5b, respectively) was observed to re-wet with time and spread back across the entirety of the array. Upon re-wetting of the electrolyte layer, a similar trend was observed in the net cathodic current density on the individual AA2024-T4 electrodes prximate to the Mg similar to what was observed during drying but in reverse. The net cathodic current density on the AA2024-T4 electrodes closest to the Mg electrode was observed to increase in magnitude from zero as the electrolyte layer re-wet and grew until a peak current density was observed (around $t = 4500$ s in Figure 4a and $t = 9400$ s in Figure 5b). The cathodic current also spread back across the AA2024-T4 array. As the electrolyte layer grew farther, wetting more AA2024-T4 electrodes, the cathodic current density on the AA2024-T4 electrodes closest to the Mg electrode at $x = 50$ μm decreased slightly and stabilized at an intermediate current density of 20 mA/cm$^2$ in NaCl and 12 mA/cm$^2$ in ASTM SOW (5000 s $< t <$ 7000 s in Figure 4a and 10,000 s $< t <$ 13,000 s in Figure 5a). Upon lowering the RH of the cabinet back down to below 40% once again, a peak in cathodic current density of 50 mA/cm$^2$ in NaCl and 20 mA/cm$^2$ in ASTM SOW on the individual AA2024-T4 electrodes closest to the Mg electrode at $x = 50$ μm was again observed (around $t = 7300$ s in Figure 4a and $t = 14{,}000$ s in Figure 5a) before the throwing power again decreased to zero.

The cathodic polarization provided by the Mg electrode was initially observed to spread across the entire width of the array indicating a TP greater than or equal to 5750 μm under a 500 ± 100 μm thick layer of 0.6 M $MgCl_2$ (Figure 7) covering the entire microelectrode array. This was indicated by a net cathodic current density greater than $10^{-6}$ A/cm$^2$ sensed on the AA2024-T4 at position = 5.75 mm in Figure 7b. Upon lowering the cabinet RH to less than 20% for more than 2 h, the electrolyte layer was visually observed to slightly decrease in thickness and a semi-solid salt cap was observed to form over the liquid electrolyte layer. $H_2$ bubbles could be seen to form and move under the salt cap and the magnitude of the cathodic current density on each AA2024-T4 electrode in the array was reduced but did not reach zero ($t_3$ in Figure 7a and 7b) and held steady at approximately $5.0 \times 10^{-4}$ A/cm$^2$ corresponding to a couple potential of −1.5 $V_{SCE}$ (assuming the 5.0 M $MgCl_2$ curve in Figure 6c). This is a marked difference from the behavior under NaCl and ASTM SOW (Figures 4 and 5) where the cathodic current density on each AA2024-T4 electrode in the array was reduced to zero upon "drying" at similar RH. The throwing power as measured by the cathodic polarization of the AA2024-T4 electrodes spanned across the entire array ($t_3$ in Figure 7a and 7b) under the salt capped electrolyte layer. After 2 h at an RH less than 20%, the RH of the cabinet was increased to roughly 93%. The salt cap was observed to dissolve and the magnitude of cathodic current density on the AA2024-T4 electrodes increased ($t_4$ in Figure 7a and 7b).

*Throwing power experimentally measured by a coupled electrode multichannel microelectrode array with the addition of a polymer layer over the Mg.*—In a fourth experiment, approximately 40 μL of 0.9 M NaCl solution was applied in a 500 ± 100 μm thick layer to the top of the polymer coated Mg/bare AA2024-T4 microelectrode

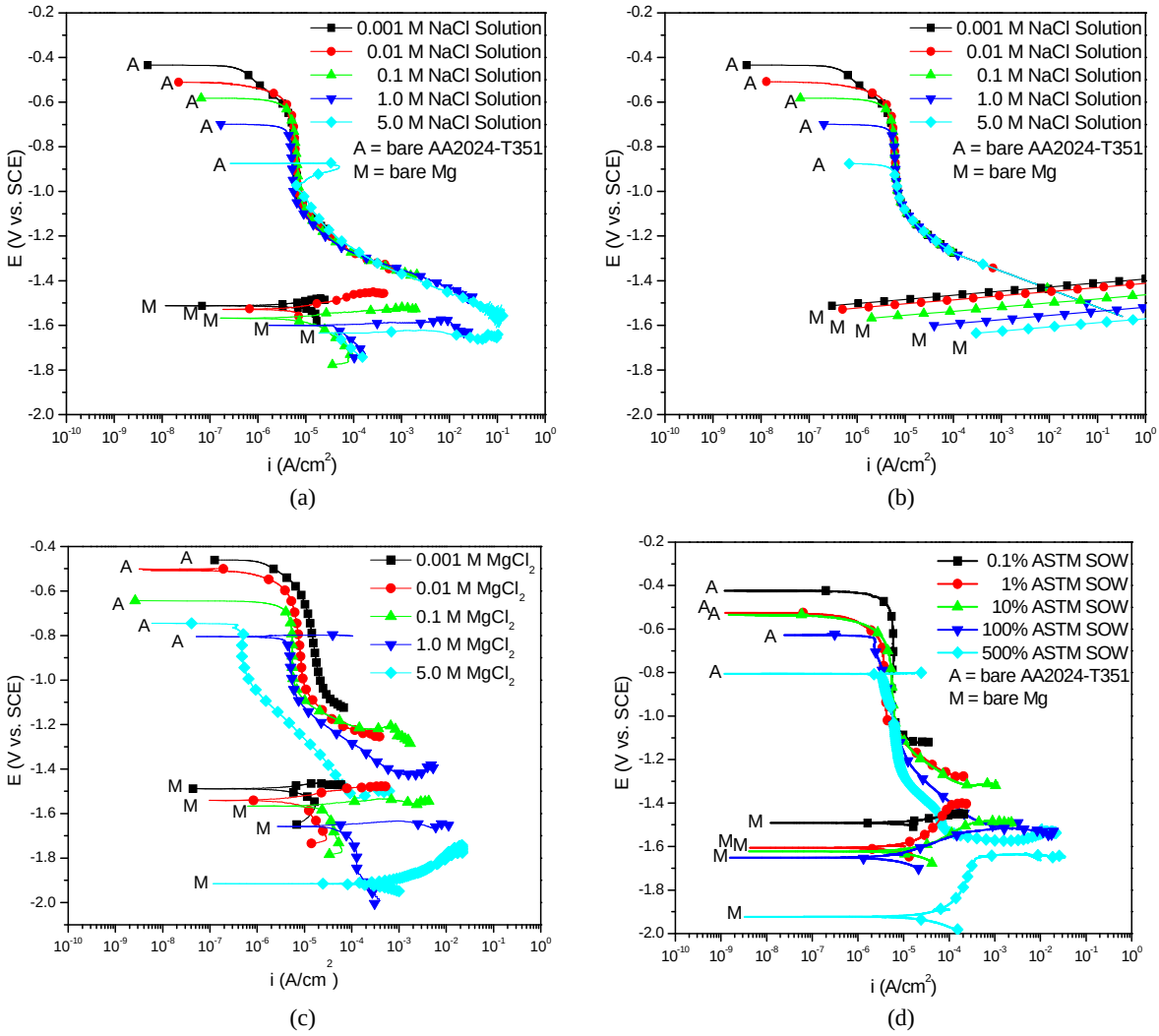


**Figure 6.** E-log(i) boundary condition data for bare high purity Mg and bare AA2024-T351 sheet in various concentrations of ambiently aerated NaCl solution. (a) experimentally obtained, full immersion polarization data in ambiently aerated NaCl solution (b) 1:1 area ration E-log(i) data for anode and cathode fitted from (a) (c) experimentally obtained, full immersion polarization data in ambiently aerated $MgCl_2$ solution (d) experimentally obtained, full immersion polarization data in quiescent, ambiently aerated ASTM Substitute Ocean Water solution.

galvanic array such that the electrolyte covered every electrode in the array. Over the course of 3 hours, the relative humidity in the cabinet was held constant at approximately 94% (Figure 8a).

The added resistance of the clear acrylic polymer (with DC impedance of $10^2 - 10^3\ \Omega \cdot m^2$ or $10^6$ to $10^7\ \Omega\text{-cm}^2$) initially mediated the sacrificial galvanic protection afforded by the Mg electrode to the AA2024-T4 electrodes in the microelectrode array ($t_1$ in Figure 8a and Figure 8b) shown by net current densities of zero on the Mg and AA2024-T4 electrodes (at $t_1$ TP = 0 μm). During this time the unprotected AA2024-T4 electrodes were freely corroding at open circuit under the 0.9 M NaCl droplet. After approximately 3000 s ($t_2$ in Figure 8), a defect formed in the clear acrylic coating, which significantly reduced the originally high ionic resistance of the polymer coating. As soon as the coating defect formed, the Mg electrode and AA2024-T4 electrodes in the microelectrode array became galvanically coupled and the throwing power extended across the entire width of the array to x = 5750 μm (at $t_2$ and $t_3$ TP = 5750 μm) for an electrolyte thickness of 500 ± 100 μm.

*Throwing power experimentally measured by a coupled electrode multichannel microelectrode array under various salt deposition densities.*—Optical micrographs of the dry array with NaCl applied at various deposition densities are shown in Figure 9. The RH in the cabinet was quickly increased to 94% to deliquesce the deposited salts (which primarily have deliquescence points below 75%). After 3 additional hours, the relative humidity in the cabinet was maintained at a constant level of approximately 94% in an attempt to equilibrate the electrolyte layer concentration with ambient temperature and humidity. Optical micrographs of the re-wet array with NaCl applied at various deposition densities are shown in Figure 9.

The recorded galvanic current profiles between the microelectrodes under various salt deposition densities at 94% RH were used to estimate the throwing power of Mg over the array. The AA2024-T4 electrode farthest away from the Mg electrode which was cathodically polarized to a cathodic current density greater than $1.0 \times 10^{-5}$ A/cm$^2$ (AA2024 couple potential $\leq -1.0\ V_{SCE}$) in magnitude was used as the indicator of throwing power distance. Triplicate exposures were conducted utilizing 10, 100, 250, and 1000 μg/cm$^2$ of both NaCl and ASTM Substitute Ocean Water salts.

The mean throwing power, as estimated by the bare Mg/bare AA2024-T4 microelectrode array, for each exposure is reported in Figure 10. A detectable throwing power could not be observed under salt deposition densities less than 250 μg/cm$^2$. This is presumably due to the relatively large 50 μm spacing between adjacent flush mounted electrodes in the 1-dimensional array geometry. The throwing power under NaCl and ASTM SOW was observed to increase with salt deposition density (Figure 10). For example, the throwing

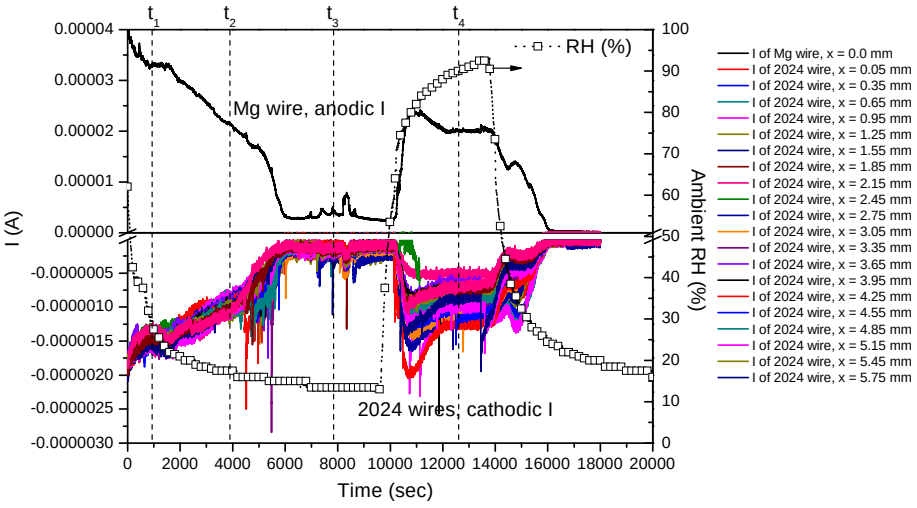


(a)

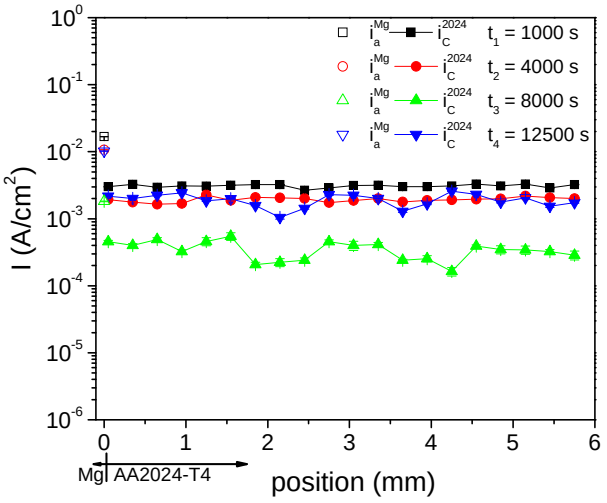


(b)

**Figure 7.** (a) Measured current and RH vs. time through each electrode and (b) average current density vs. position on the bare Mg/AA2024-T4 microelectrode array during an episodic wetting and drying event under 0.6 M $MgCl_2$ solution.

power at 94% RH was estimated to be $< 50$ μm for 100 μg/cm$^2$ of ASTM SOW. However, the throwing power was $\geq 2000$ μm for 1000 μg/cm$^2$ of ASTM SOW. Due to variation in the particular location of deposited salt crystals and the variation in the location of individual droplets, there is significant variability of these estimations between runs (error bars in Figure 10). Additionally, the throwing power for ASTM SOW was observed to be greater compared to NaCl. This is possibly due to the presence of $MgCl_2$ and $CaCl_2$ in the ASTM SOW which equilibrates at 94% RH to lower concentrations (hence larger droplet volume) than NaCl at a given RH causing larger droplets to form and coalesce. Additionally, it was noticed that the dry SOW (after wet application and subsequent drying) appeared to have a greater dispersion of salt crystals across the surface of the array possibly due to salt species segregation upon drying of the SOW solution.[41,42]

The galvanic current between the microelectrodes under 1000 μg/cm$^2$ of NaCl deposits is shown in Figure 11a and a corresponding optical micrograph and color coded diagram taken at the time of maximum throwing power during this exposure are shown in Figure 11b. The color coded array diagram in Figure 11b indicates that the second AA2024-T4 electrode away from the Mg electrode ($x = 350$ μm) was the farthest AA2024-T4 electrode cathodically polarized by being galvanically coupled to the Mg electrode. This resulted in an estimation of throwing power of 350 μm. 350 μm was the shortest distance from the closest edge of the Mg electrode to the closest edge of the furthest away, cathodically polarized AA2024-T4 electrode.

The recorded galvanic current between the microelectrodes under 1000 μg/cm$^2$ of ASTM SOW salt is shown in Figure 12a and a corresponding optical micrograph and color coded diagram taken at the time of maximum throwing power during this exposure are shown in Figure 12b. The color coded array diagram in Figure 12b indicates that the AA2024-T4 electrode 3950 μm away from the Mg electrode was cathodically polarized. This resulted in an estimation throwing power of 3950 μm. 3950 μm was the shortest distance from the closest edge of the Mg electrode to the closest edge of the farthest cathodically polarized AA2024-T4 electrode. In the optical micrograph in Figure 12, it can be seen that separate droplets coalesced into a larger droplet which was "C" shaped such that it covered the Mg electrode, AA2024-T351 electrodes at $x = 50$ to 1550 μm and also electrodes from 3050 to 3950 μm but not the electrodes between 1550 and 3050 μm away from the Mg.

## Discussion

*Important parameters governing galvanic throwing power of MgRP over bare AA2024-T351.*— The experiments conducted in this work utilizing a galvanic couple multichannel microelectrode array shed light on how various aspects of MgRP coating formulation and properties of the exposure environment combine to produce the

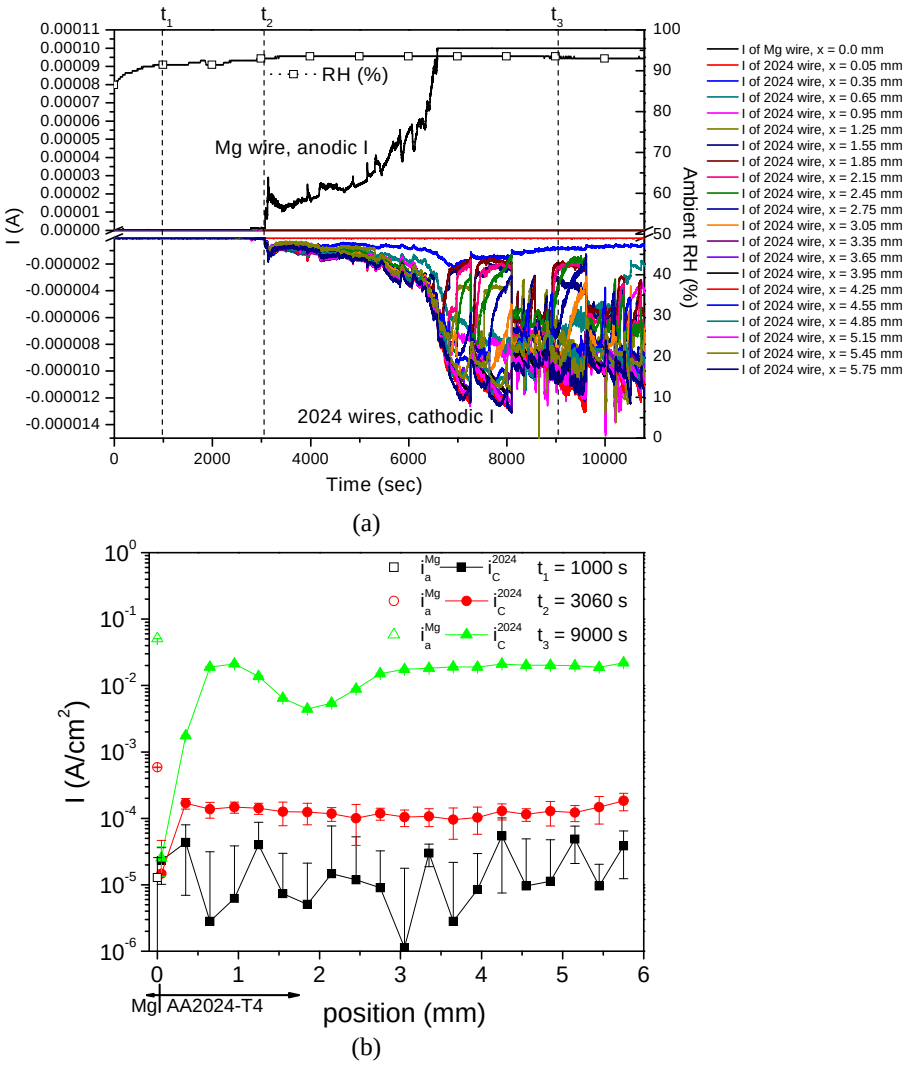


**Figure 8.** (a) Measured current and RH vs. time through each electrode and (b) average current density vs. position on the polymer-coated-Mg/bare AA2024-T4 microelectrode array exposed to 93% RH under 0.9 M NaCl solution. The polymer developed defect after $t_2$.

current and potential distribution and resulting galvanic throwing power for protection of the AA2024-T351 across a scribe or scratch. In both cases, the cathodic current density was greater near the scratch/coating interface and could be leveled or made more uniform only by a large polymer resistance and a thick electrolyte layer. This was because the electrolye resistance became a less dominant factor than the high ohmic resistance of the organic coating. For instance, resistivity of the polymer was $\sim 10^9$ ohm-cm versus 25 ohm-cm for 0.6 M NaCl.

*Effect of electrolyte layer on the galvanic throwing power in the MgRP/AA2024-T351 system.*—The chemistry, thickness, and geometric area of coverage of the electrolyte layer were all shown, with an instrumented galvanic microelectrode array, to play an important role in governing the galvanic throwing power of Mg across a simulated defect or scratch of bare AA2024-T351. The chemistry (chemical species present and concentration) of the electrolyte layer (whether deposited by precipitation, immersion, or deliquescence of deposited salts) was shown with the microelectrode array to accurately govern the electrochemical E-i boundary conditions (Figure 6) of the anode and cathode when the polymer resistance was zero. As evidence of this, the galvanic current on each anode and cathode in the microelectrode array (Figures 4, 5, and 7) was in qualitative agreement with estimations from a mixed potential model (Figure 13) based on the electrochemical E-i boundary conditions shown in Figure 6 and finite ohmic voltages between anodes and cathodes. Increasing the NaCl solution concentration by an order of magnitude by drying (in which the electrolyte is assumed to saturate just before drying) resulted in an increase in the galvanic current density by almost one order of magnitude (Figures 4, 5, and 7).[43–45]

The chemical species in the electrolyte also dictate the deliquescence and equilibrium behavior of the electrolyte layer exposed to various ambient RH. For example, when the microelectrode array was exposed under continuous, thin electrolyte layers of pure $MgCl_2$, rather than NaCl or ASTM Substitute Ocean Water, the electrolyte layer did not completely dry at low RH (Figure 7). In turn the galvanic interaction did not cease because full drying did not occur at low RH.[21,22]

In conjunction with electrolyte chemistry, the thickness and geometric area of coverage of the electrolyte layer (which are all influenced by deposition density, immersion condition, or RH and deliquescence of deposited salts shown in Figures 1 and 9) controls the amount of area of both the anode and the cathode that can be galvanically coupled together. A sacrificial anode (or a sacrificial coating such as an MgRP) can only protect the area of a cathode (scratch or scribe exposing bare AA2024-T351 substrate), of which it is both electrically and ionically connected. In exposures of the microelectrode array under continuous, thin electrolyte layers ($t_1$ in Figures 4, 5, and 7) the throwing power extended across the entire array. However, whenever the electrolyte became tortuous, either due to drying ($t_3$ in Figures 4, 5, and) or due to the formation of isolated droplets due to low initial salt deposition density at a given RH (Figures 9, 10, 11, and 12) the throwing power

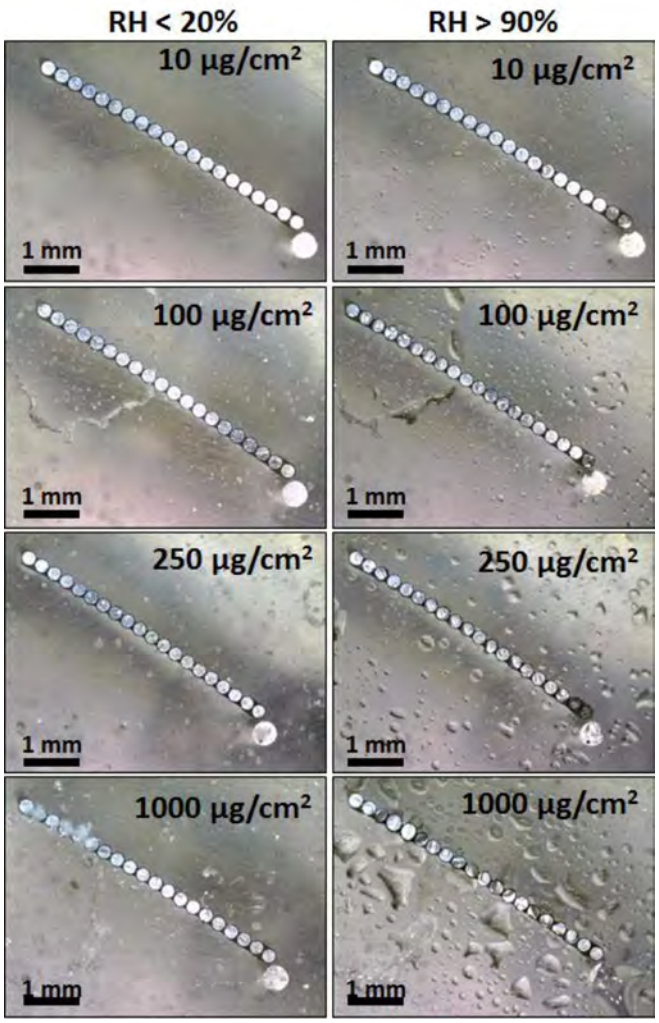


**Figure 9.** Optical micrographs of various deposition densities of NaCl on a microelectrode array consisting of one 500 µm diameter 99.9% Mg wire and twenty isolated, 254 µm diameter AA2024-T4 wires in the dry (RH < 20%) and wet (RH > 90%) condition.

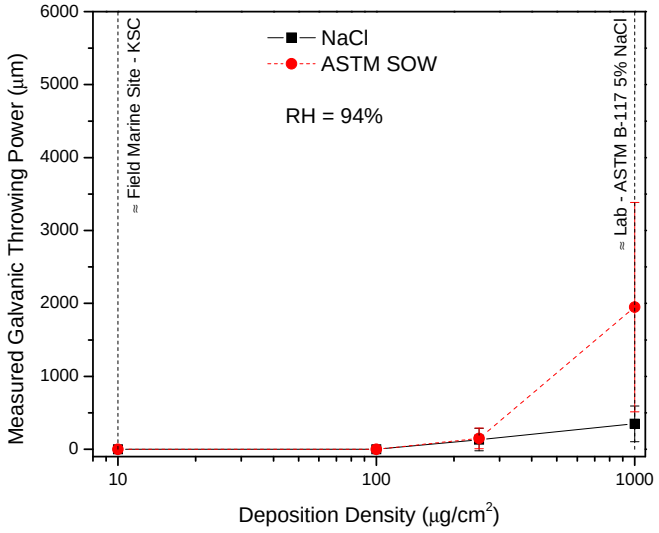


**Figure 10.** Observed throwing power of Mg under various deposition densities of NaCl and ASTM SOW applied via a spray bottle application method at equilibrium in 94% RH.

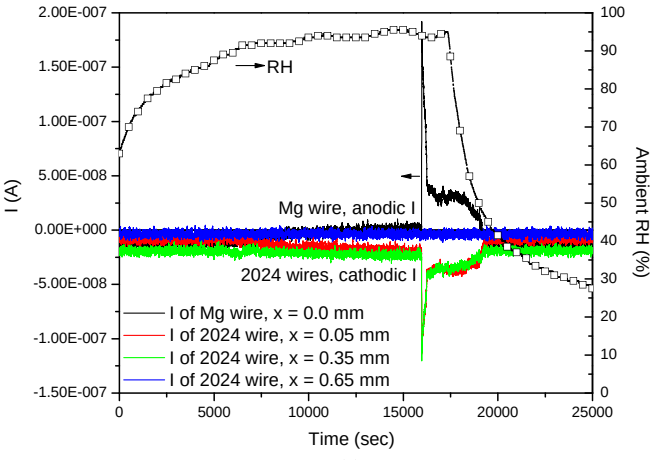


(a)

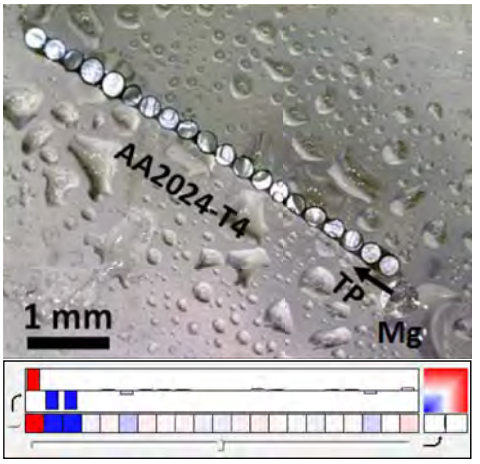


(b)

**Figure 11.** (a) Measured current and RH and (b) optical image of the bare-Mg/bare AA2024-T4 microelectrode array with 1000 µg/cm$^2$ NaCl deposited by salt spray and allowed to equilibrate at 94% RH for at least 3 h. In the color map dark red indicates an anodic current $\geq 1 \times 10^{-5}$ A/cm$^2$ and dark blue indicates a cathodic current of $\leq -1 \times 10^{-5}$ A/cm$^2$. White color indicates a net current of zero.

was limited by an increasingly tortuous electrolyte geometry which hindered or complicated the ionically conductive path even though the ionic conductivity of the drop increased (shown schematically in Figure 14a).

*Effect of organic polymers on the galvanic throwing power in the MgRP/AA2024-T351 system.*—The role of the polymer layers in the MgRP/AA2024-T351 system is extremely important and twofold. The primer and topcoat polymers both (1) act as a barrier to protect the Mg pigment from rapid self-corrosion and (2) mediate the cathodic protection potential provided to the AA2024-T351 substrate by the Mg pigment. This is brought about due to the sum of ohmic resistance of the polymer binder, geometry of the buried pigment particles, and the ohmic resistance of the ionic conducting electrolyte. The combined effect will be the subject of finite element modeling in future work to address the complex scratch geometry and complex galvanic current paths.

Mediation of extremely negative cathodic potentials over the 2024 can avoid detrimental cathodic corrosion of the AA2024-T351 substrate[46–48] and subsequent blistering by rapid $H_2$ evolution at cathodic sites.[10] The mediation is brought about through insertion of a large ohmic resistance and voltage in the galvanic couple which in accordance with mixed potential theory produces a difference in the interfacial potentials across the double layers of the Mg and the

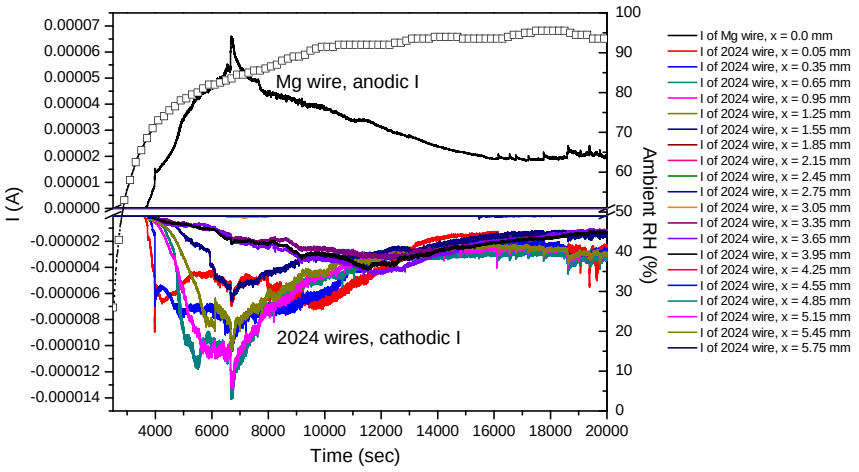


(a)

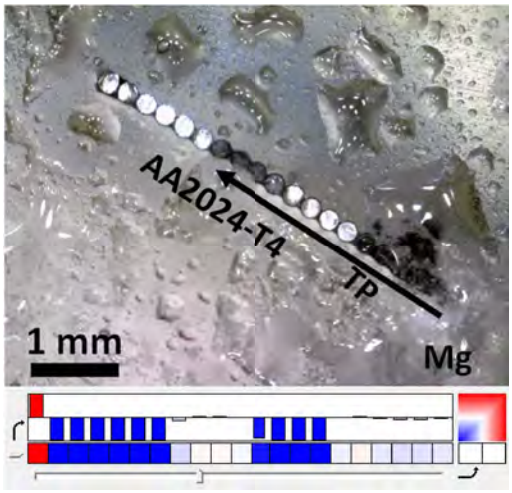


(b)

**Figure 12.** (a) Measured current and RH and (b) optical of the bare-Mg/ bare AA2024-T4 microelectrode array with 1000 $\mu$g/cm$^2$ ASTM SOW salt deposited by salt spray and allowed to equilibrate at 94% RH for at least 3 h. In the color map dark red indicates an anodic current $\geq 1 \times 10^{-5}$ A/cm$^2$ and dark blue indicates a cathodic current of $\leq -1 \times 10^{-5}$ A/cm$^2$. White color indicates a net current of zero.

2024, respectively. It has been shown in the past that AA2024-T351 polarized cathodically to – 1.5 V vs. SCE in aerated NaCl solution dissolves at a rate as high as 4 mA/cm$^2$. However, the same alloy was shown to avoid significant cathodic corrosion when cathodically polarized above −1.1 V vs. SCE.[47] Recent, independant field and laboratory studies of commercial MgRP products did not report any observations of cathodic corrosion of the AA2024-T351 substrate after prolonged environmental exposure and in the case of high resistance topcoated systems. Moreover, depletion of Mg pigment from the coating was significantly mediated.[12,13,49–52] Such results highlight the importance of the the primer and topcoat polymers in controlling the coating performance. The precise nature of this mediation process is best addressed in finite element modeling of the current and potential distribution accounting for the coating resistance in series with the electroltye resistance.

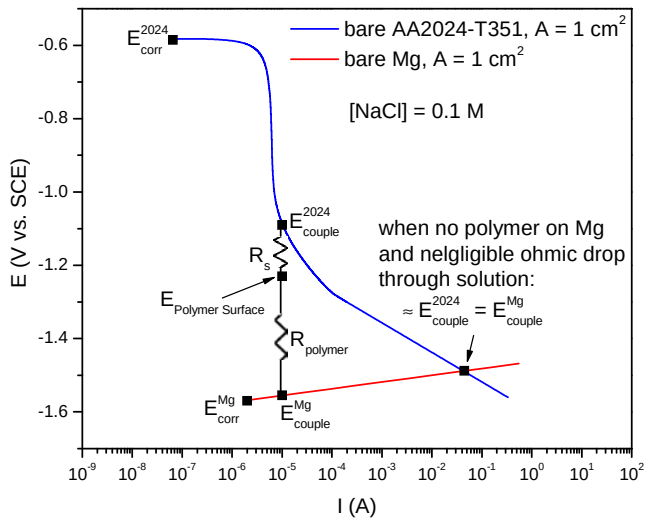


**Figure 13.** Mixed potential model depicting a galvanic couple between AA2024-T351 and polymer coated Mg.

When a quick-drying, acrylic polymer with similar barrier properties to that of a commercial MgRP was applied to the surface of the Mg electrode in the Mg/AA2024-T4 microelectrode array, the added resistance of the polymer mediated the sacrificial galvanic protection afforded by the Mg electrode to the AA2024-T4 electrodes in the microelectrode array ($t_1$ in Figure 8a and Figure 8b), shown by net current densities of zero on the Mg and AA2024-T4 electrodes (at $t_1$ TP = 0 $\mu$m) due to the large ohmic resistance of the intact polymer. For this reason, in the MgRP system, besides any geometric limitations brought about by a discontinuous ionic pathway, the electrical and ionic resistances of any pretreatment layers, primer formulations, or topcoat systems appears to be the most important tunable factor at the disposal of the coating designer governing the galvanic protection function of the MgRP pertaining to throwing power and self-corrosion of the Mg pigment. However, the polymer resistance levels the potential and current distribution across the scratch of exposed AA2024 at the expense of the galvanic current which is lowered (Figure 8).

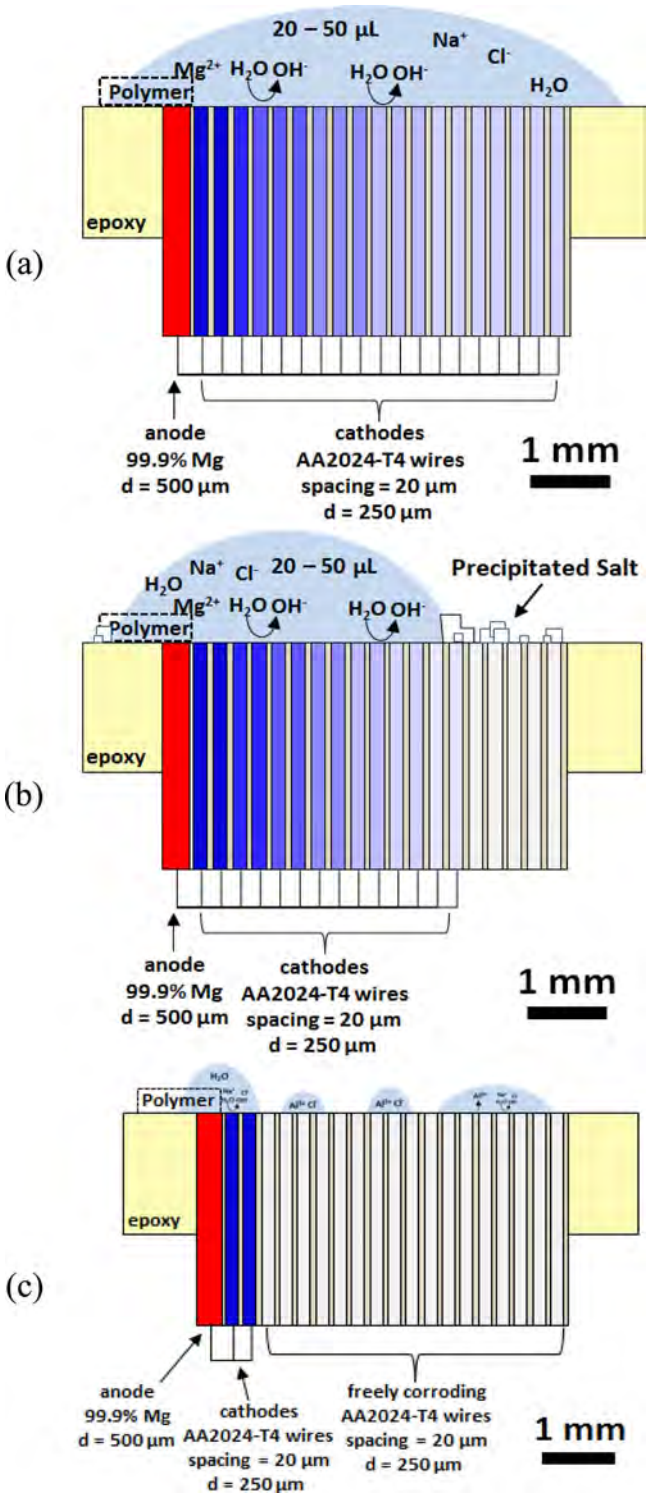


**Figure 14.** Hypothetical schematic depicting the galvanic couple interaction between microelectrodes in the Mg/AA2024-T4 array under (a) continuous (thin layer) and (b) drying (shrinking) continuous thin-layer and (c) discontinuous electrolyte (droplet) layer which can occur during re-wetting of deposited dried salts or droplet deposition.

The ohmic resistance brought about by a simulated primer and topcoat polymers are shown to severely mediate the throwing power of the Mg over the AA2024 scribe (Figure 10). In the actual coating scenario, this is presumed to be accurate except for locations very proximate to the edge of the coating where there exists a small area of bare Mg exposed to solution next to the cross-section or wall of the scratch where $R_{polymer}$ is considerably less than the path through the covering primer and top coat plane.

*Important limitations of the microelectrode galvanic array – future work.*—The microelectrode galvanic array proved to be an extremely useful tool to examine the galvanic throwing power of a simulated MgRP / AA2024-T351 system during simulated atmospheric exposure. However, there are many improvements which could be made to the microelectrode array that would improve the correlation to real environmental exposure. The microelectrode array would be more analogous to the real MgRP/AA2024-T351 system if the microelectrodes were embedded in AA2024-T351 sheet instead of mounted in epoxy polymer and a MgRP coating could be utilized in place of the Mg electrode. It is well known that the wettability of the surface of aluminum and its oxides is high compared to that of polished organic epoxy polymers. This difference would likely lead to greater throwing powers being observed on an array embedded in an AA2024-T351 panel as compared to those observed on the epoxy embedded array used in this work.

## Conclusions

- The interface between the bare Mg and bare AA2024 always experienced the greatest cathodic current density. When the resistance of the polymer layer was added, which dominated the electrolyte path resistance, the cathodic current density across all of the AA2024 electrodes was relatively equal in magnitude.
- The chemistry, thickness, and geometric area of coverage of the electrolyte layer were all shown to be important in governing the galvanic throwing power of Mg across a simulated defect or scratch consisting of bare AA2024-T351 in simulated atmospheric exposure.
- Increasing the NaCl solution concentration by an order of magnitude results in an increase in the galvanic current density over the AA2024 by almost one order of magnitude.
- During drying, the net cathodic current density on the AA2024-T4 electrodes closest to the Mg electrode increased to a maximum, presumably due to the combined effects of the increasing electrolyte concentration and the decreasing area of the active cathode relative to a fixed anode area combined with effects on the E-I interface behavior. Upon further drying, the net cathodic current density on the AA2024-T4 electrodes closest to the Mg electrode were then observed to decrease in magnitude to zero as the effect of the increasingly thin and tortuous electrolyte geometry reduced the ionically conductive path despite the increase in concentration of NaCl. Upon re-wetting of the electrolyte layer, a similar trend was observed in the net cathodic current density on the individual AA2024-T4 electrodes closest to the Mg similar to that observed during drying but in reverse.
- The exact identity of the chemical species in the electrolyte also dictate the deliquescence and equilibrium behavior of the electrolyte layer exposed to various ambient RH and temperature. For instance, when the microelectrode array was exposed under continuous, thin electrolyte layers of pure $MgCl_2$, in contrast with behavior in NaCl or ASTM Substitute Ocean Water, the electrolyte layer did not completely dry at low RH and residual cathodic protection of AA2024-T351 was observed.
- In exposures of the microelectrode array under continuous, thin electrolyte layers, the throwing power extended across the entire 5.75 mm wide array. However, whenever the electrolyte became tortuous, either due to drying or due to the formation of isolated droplets due to low initial salt deposition density, the throwing power was limited to less than 5.75 mm (over the entire range of >5.75 mm down to 0 mm during a given wet/dry cycle) by an increasingly tortuous electrolyte geometry which reduced the ionically conductive path length.
- When a polymer with similar barrier properties to that of a commercial MgRP topcoat system was applied to the surface of the Mg electrode in the Mg/AA2024-T4 microelectrode array, the added resistance of the polymer significantly mediated the sacrificial galvanic protection afforded by the Mg electrode to the AA2024-T4 electrodes

and resulted in a measured throwing power of only 50 μm prior to coating barrier degradation.

## Acknowledgments

This work was supported by the US DoD OUSD Corrosion University Pilot Program under the direction of Daniel Dunmire and by the National Science Foundation under NSF DMR #0906663. This material is based on research sponsored by the US Air Force Academy under agreement number FA7000-13-2-0020. The U.S. Government is authorized to reproduce and distribute reprints for Governmental purposes notwithstanding any copyright notation thereon. The views and conclusions contained herein are those of the authors and should not be interpreted as necessarily representing the official policies or endorsements, either expressed or implied, of the US Air Force Academy or the U.S. Government NRL/JA/7330-2014-2175.

## References

1. S. S. Pathak, M. D. Blanton, S. K. Mendon, and J. W. Rawlins, *Corros Sci*, **52**(4), 1453 (2010).
2. G. P. Bierwagen, D. E. Tallman, M. Nanna, D. Battocchi, A. Stamness, and V. J. Gelling, *Abstr Pap Am Chem S*, **228** U360 (2004).
3. A. Simoes, D. Battocchi, D. Tallman, and G. Bierwagen, *Prog Org Coat*, **63**(3), 260 (2008).
4. D. Battocchi, A. M. Simoes, D. E. Tallman, and G. P. Bierwagen, *Corros Sci*, **48**(8), 2226 (2006).
5. D. Battocchi, A. M. Simoes, D. E. Tallman, and G. P. Bierwagen, *Corros Sci*, **48**(5), 1292 (2006).
6. H. Xu, D. Battocchi, D. E. Tallman, and G. P. Bierwagen, *Corrosion*, **65**(5), 318 (2009).
7. G. Bierwagen, D. Battocchi, A. Simoes, A. Stamness, and D. Tallman, *Prog Org Coat*, **59**(3), 172 (2007).
8. A. D. King and J. R. Scully, *Corrosion*, **67**(5), 05500401 (2011).
9. B. Maier and G. S. Frankel, *Corrosion*, **67**(5), 055001 (2011).
10. A. D. King and J. R. Scully, in *NACE DoD 2011 Conference Proceedings*, Palm Springs, CA, 2011.
11. J. Nie, M. C. Yan, J. Wang, D. E. Tallman, D. Battocchi, and G. P. Bierwagen, *ECS Transactions*, **24**(1), 261 (2010).
12. A. D. King, B. Kannan, and J. R. Scully, *Corrosion*, **70**(5), (2014).
13. A. D. King, B. Kannan, and J. R. Scully, *Corrosion*, **70**(5), (2014).
14. D. H. Wang, D. Battocchi, K. N. Allahar, S. Balbyshev, and G. P. Bierwagen, *Corros Sci*, **52**(2), 441 (2010).
15. M. E. Nanna and G. P. Bierwagen, *Jct Research*, **1**(2), 69 (2004).
16. F. Presuel-Moreno, M. A. Jakab, N. Tailleart, M. Goldman, and J. R. Scully, *Mater Today*, **11**(10), 14 (2008).
17. F. J. Presuel-Moreno, M. E. Goldman, R. G. Kelly, and J. R. Scully, *J Electrochem Soc*, **152**(8), B302 (2005).
18. F. J. Presuel-Moreno, H. Wang, M. A. Jakab, R. G. Kelly, and J. R. Scully, *J Electrochem Soc*, **153**(11), B486 (2006).
19. J. R. Scully, F. Presuel-Moreno, M. Goldman, R. G. Kelly, and N. Tailleart, *Corrosion*, **64**(3), 210 (2008).
20. F. Presuel-Moreno, H. Wang, M. Jakab, and R. Kelly, *Corrosion*, **62**, 251 (2006).
21. E. Schindelholz, B. E. Risteen, and R. G. Kelly, *J Electrochem Soc*, **161**(10), C450 (2014).
22. E. Schindelholz, B. E. Risteen, and R. G. Kelly, *J Electrochem Soc*, **161**(10), C460 (2014).
23. B. E. Risteen, E. Schindelholz, and R. G. Kelly, *J Electrochem Soc*, **161**(14), C580 (2014).
24. C. Deslouis, A. Doncescu, D. Festy, O. Gil, V. Maillot, S. Touzain, and B. Tribollet, *Electrochemical Methods in Corrosion Research Vi, Pts 1 and 2*, **289**(2), 1163 (1998).
25. C. Deslouis, D. Festy, O. Gil, G. Rius, S. Touzain, and B. Tribollet, *Electrochim Acta*, **43**(12–13), 1891 (1998).
26. R. A. Humble, *Corrosion*, **4**, 358 (1948).
27. R. U. Lee and J. R. Ambrose, *Corrosion*, **44**(12), 887 (1988).
28. F. G. Liu, S. R. Wu, and C. S. Lu, *Corros Eng Sci Techn*, **46**(5), 611 (2011).
29. C. Rousseau, F. Baraud, L. Leleyter, M. Jeannin, and O. Gil, *Corros Sci*, **52**(6), 2206 (2010).
30. C. Barchiche, C. Deslouis, D. Festy, O. Gil, P. Refait, S. Touzain, and B. Tribollet, *Electrochim Acta*, **48**(12), 1645 (2003).
31. C. Deslouis, D. Festy, O. Gil, V. Maillot, S. Touzain, and B. Tribollet, *Electrochim Acta*, **45**(11), 1837 (2000).
32. Y. L. Cheng, Z. Zhang, F. H. Cao, J. F. Li, J. Q. Zhang, J. M. Wang, and C. N. Cao, *Corros Sci*, **46**(7), 1649 (2004).
33. M. A. Jakab, D. A. Little, and J. R. Scully, *J Electrochem Soc*, **152**(8), B311 (2005).
34. J. R. Scully, *J Electrochem Soc*, **136**(4), 979 (1989).
35. M. Kendig, F. Mansfeld, and S. Tsai, *Corros Sci*, **23**(4), 317 (1983).
36. M. W. Kendig, F. Mansfeld, and C. H. Tsai, *Corrosion*, **47**(12), 964 (1991).
37. F. Mansfeld, *Electrochim Acta*, **39**(10), 1451 (1994).
38. F. Mansfeld, *Electrochim Acta*, **38**(14), 1891 (1993).
39. F. Mansfeld, L. T. Han, C. C. Lee, and G. Zhang, *Electrochim Acta*, **43**(19–20), 2933 (1998).
40. F. Mansfeld, M. W. Kendig, and S. Tsai, *Corrosion*, **38**(9), 478 (1982).
41. I. S. Cole, T. H. Muster, D. Lau, N. Wright, and N. S. Azmat, *J Electrochem Soc*, **157**(6), C213 (2010).
42. I. S. Cole, T. H. Muster, S. A. Furman, N. Wright, and A. Bradbury, *J Electrochem Soc*, **155**(5), C244 (2008).
43. M. Stratmann and H. Streckel, *Corros Sci*, **30**(6–7), 681 (1990).
44. M. Stratmann and H. Streckel, *Corros Sci*, **30**(6–7), 697 (1990).
45. M. Stratmann, H. Streckel, K. T. Kim, and S. Crockett, *Corros Sci*, **30**(6–7), 715 (1990).
46. B. P. Caldwell and V. J. Albano, *Transactions of The Electrochemical Society*, **76**(1), 271 (1939).
47. M. Mokaddem, P. Volovitch, F. Rechou, R. Oltra, and K. Ogle, *Electrochim Acta*, **55**(11), 3779 (2010).
48. M. Serdechnova, P. Volovitch, F. Brisset, and K. Ogle, *Electrochim Acta*, **124**(0), 9 (2014).
49. W. H. Abbott, *Personal correspondence with Mr. William Abbott of Battelle Memorial Institute* (2013).
50. W. H. Abbott, in *NACE DoD 2011 Conference Proceedings*, Palm Springs, CA, 2011.
51. W. H. Abbott, H. O. Pate, and F. Fernandez, in *NACE DoD 2013 Cyber Conference Proceedings*, 2013.
52. C. Matzdorf, *Personal correspondence with Mr. Craig Matzdorf of U. S. Naval Air Systems Command* (2013).